Available online at www.sciencedirect.com
ScienceDirect
Polymer 48 (2007) 6018–6028
polymer
www.elsevier.com/locate/polymer

Isothermal crystallization of poly(glycolic acid-*alt*-6-hydroxyhexanoic acid) studied by DSC and real time synchrotron SAXS/WAXD

Meritxell Martínez-Palau, Lourdes Franco, Jordi Puiggalí*

Departament d'Enginyeria Química, Universitat Politècnica de Catalunya, Av. Diagonal 647, E-08028 Barcelona, Spain

Received 29 June 2007; accepted 2 August 2007
Available online 8 August 2007

Abstract

The thermal properties and the isothermal hot crystallization behavior of a new regular polyester constituted of glycolic acid and 6-hydroxyhexanoic acid units were studied by differential scanning calorimetry (DSC). The morphological development during isothermal crystallization was also investigated using simultaneous small-angle X-ray scattering (SAXS) and wide-angle X-ray diffraction (WAXD) techniques with synchrotron radiation. A crystalline–amorphous two-phase lamellar system was assumed and interpreted using correlation functions.

Kinetic parameters deduced from the Avrami analysis indicated a three-dimensional spherulitic growth from heterogeneous nuclei, whereas optical micrographs revealed the formation of small spherulites with a negative birefringence and a fibrillar texture. The Lauritzen and Hoffman analysis of crystallization regimes was performed taking into account the kinetic constants of the overall crystallization process deduced from DSC and also the reciprocal crystallization halftimes evaluated by means of DSC, SAXS and WAXD experiments. Data were consistent with a single crystallization regime and yielded similar values for the transport activation energy and the nucleation constant in all cases.

The evolution of long period and lamellar thickness was evaluated during crystallization. Changes with both crystallization time and crystallization temperature were significant.

Keywords: Polyester; Glycolic acid; Isothermal crystallization

1. Introduction

The development of new biodegradable polymers is a subject of great interest due to their potential applications such as those found in the biomedical field. Thus, biodegradable polymers are currently being investigated for use in wound closure (sutures, staples); orthopedic fixation devices (pins, rods, screws, tacks, ligaments); dental, cardiovascular and intestinal applications; drug delivery systems; and matrices for cell culture [1–3]. Most of the commercially available biodegradable devices are polyesters, for example the homopolymer and copolymers of glycolide [4–6]. The latter are usually prepared by ring opening polymerization of glycolide and appropriate cyclic comonomers, and consequently have a random microstructure that hinders their crystallization.

A new method of synthesis has recently been proposed for obtaining alternating copolymers of glycolic acid and ω-amino acids [7,8] or ω-hydroxy acids [9]. This method is based on a thermal polycondensation with formation of a metal salt as a driving force (Scheme 1a) and allows a highly porous material to be obtained after water washing. New polymers can cover a wide range of properties since two different families (polyesters and poly(ester amide)s) with a variable methylene content are involved.

It is well known that the rate of degradation is a function of the degree of crystallinity as well as a morphological feature. Thus, degradation occurs at different rates through the amorphous and crystalline regions of the sample [10]. Moreover, morphological variables at the lamella level may play a significant role in the degradation mechanism [11,12].

* Corresponding author. Tel.: +34 93 4016684; fax: +34 93 4010978.
E-mail address: jordi.puiggali@upc.es (J. Puiggalí).

0032-3861/$ - see front matter © 2007 Elsevier Ltd. All rights reserved.
doi:10.1016/j.polymer.2007.08.001

(a)

$$ClCH_2CONH(CH_2)_{n-1}COO^-M^+ \xrightarrow{\Delta} -[OCH_2CONH(CH_2)_{n-1}CO]_x- + x\,MCl$$

Poly(ester amide)

$$Cl(CH_2)_3COOCH_2COO^-M^+ \xrightarrow{\Delta} -[O(CH_2)_3COOCH_2CO]_x- + x\,MCl$$

Polyester

(b)

$ClCH_2COCl + HO(CH_2)_5COOH$[1]

$\downarrow CHCl_3$

$ClCH_2COO(CH_2)_5COOH$

$\downarrow KHCO_3 \mid H_2O$

$ClCH_2COO(CH_2)_5COO^-K^+$

$\downarrow$ Vacuum, Δ

$-[OCH_2COO(CH_2)_5CO]_x- + x\,KCl$

Poly(Glc-*alt*-6HH)

[1] Obtained by basic hydrolysis of caprolactone

Scheme 1.

This work focuses on the study of the isothermal crystallization behavior of the new alternating polyester (abbreviated as poly(Glc-*alt*-6HH)) constituted of glycolic acid and 6-hydroxyhexanoic acid, which are two of the most common units in commercial biodegradable polymers. Changes at both lamellar and unit cell levels will be evaluated using simultaneous small-angle X-ray scattering (SAXS) and wide-angle X-ray diffraction (WAXD) techniques with synchrotron radiation.

2. Experimental section

Poly(Glc-*alt*-6HH) was synthesized by thermal polyesterification of the potassium salt of 6-(2-chloroacetate)hexanoic acid with an 80% yield (Scheme 1b). The intrinsic viscosity measured in dichloroacetic acid at 25 °C was 0.80 dL/g. The weight average molecular weight and polydispersity index estimated by GPC were 28,600 g/mol and 2.07, respectively.

Thermal analysis was performed by differential scanning calorimetry (DSC) with a Thermal Analysis Q100 instrument with T_{zero} technology and equipped with a refrigerated cooling system (RCS) which operates from −90 °C to 550 °C using a two-stage, closed, evaporative refrigerator system. Indium metal was employed for enthalpy and temperature calibration. The T_{zero} calibration requested two experiments: the first was done without samples and the second one was performed with sapphire disks. Thermal characterization was carried out following a protocol that involves a first heating run of the sample directly obtained from polymerization, a cooling run from the melt state, a second heating run of the melt-crystallized sample, and finally a third heating run with the sample previously quenched to −90 °C from the melt. Heating and cooling runs were performed at 20 °C/min and −10 °C/min, respectively. Samples weight ranged between 6 mg and 8 mg and all operations were performed under nitrogen. Hot-crystallization studies were conducted with samples held in the melt state for 5 min to remove any thermal history and were then quickly quenched to the selected isothermal crystallization temperature. The endothermic curves of heat flow as a function of time were recorded and analyzed.

Spherulites were grown over a cover slide from uniform molten thin films, which were produced by evaporation of a dilute polymer solution in hexafluoroisopropanol (1 mg/mL). Samples were isothermally crystallized at different temperatures below the melting point. A Linkam THMS 600 hot stage mounted on an Olympus BX5 polarizing microscope was used. Optical photographs were taken using an Olympus C3030Z digital camera. A first-order red tint plate was employed to determine the sign of spherulite birefringence under crossed polarizers.

The simultaneous time-resolved SAXS/WAXD experiments were carried out on beamline BM16 of the European Synchrotron Radiation Facility of Grenoble. The beam was monochromatized to a wavelength of 0.098 nm. The capillary with the sample was held in a Linkam hot stage with temperature control within 0.1 °C. SAXS and WAXD profiles were acquired simultaneously during cooling experiments in time frames of 14 s. Two linear position-sensitive detectors were used [13]: the SAXS detector was calibrated using different orders of diffraction from silver behenate, whereas the WAXD detector was calibrated with the different diffractions of a standard of an alumina (Al_2O_3) sample. The diffraction profiles were normalized to the beam intensity and corrected considering the empty sample background. Deconvolution of WAXD peaks was performed with the PeakFit v4 program by Jandel Scientific Software using a mathematical function known as ''Gaussian and Lorentzian area''. Calculation of the correlation function and the corresponding parameters was performed using the CORFUNC program [14] provided by the Collaborative Computational Project 13 for Fibre Diffraction/Non-Crystalline Diffraction, CCP13.

3. Results and discussion

3.1. Thermal behavior of poly(Glc-alt-6HH)

A typical DSC characterization of poly(Glc-*alt*-6HH) is shown in Fig. 1, where traces corresponding to different scans are plotted. The polymer is characterized by a predominant melting peak close to 64 °C that is observed in all different heating runs. However, hot crystallized samples also show a minor peak at a lower temperature and an exotherm just before the last melting peak, which is indicative of a lamellar reorganization. This recrystallization is also observed as a broader exotherm in the heating run of a quenched sample which, in addition, has a broad melting peak and suggests continuous melt and recrystallization processes on heating. Melting enthalpies of melt and cold crystallized samples are practically identical (6.4 kJ/mol and 6.5 kJ/mol, respectively, once the exothermic contribution is subtracted) and significantly lower than that measured from the solution crystallized

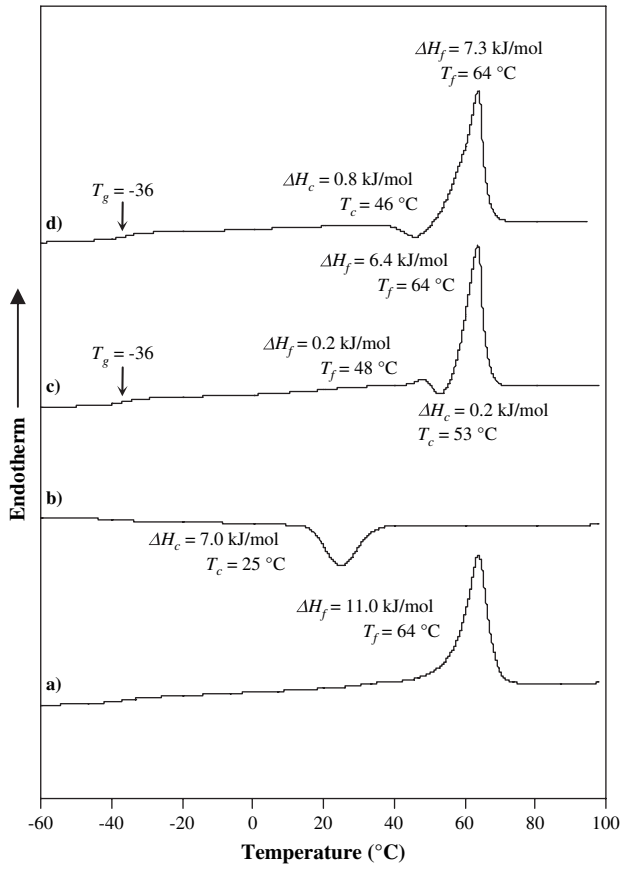

Fig. 1. DSC scans performed with poly(Glc-*alt*-6HH): (a) heating run (20 °C/min) of the original sample, (b) cooling run (10 °C/min) after keeping the sample in the melt state for 5 min, (c) heating run (20 °C/min) of the above non-isothermally crystallized sample, and (d) heating run (20 °C/min) of the previously quenched sample from the melt.

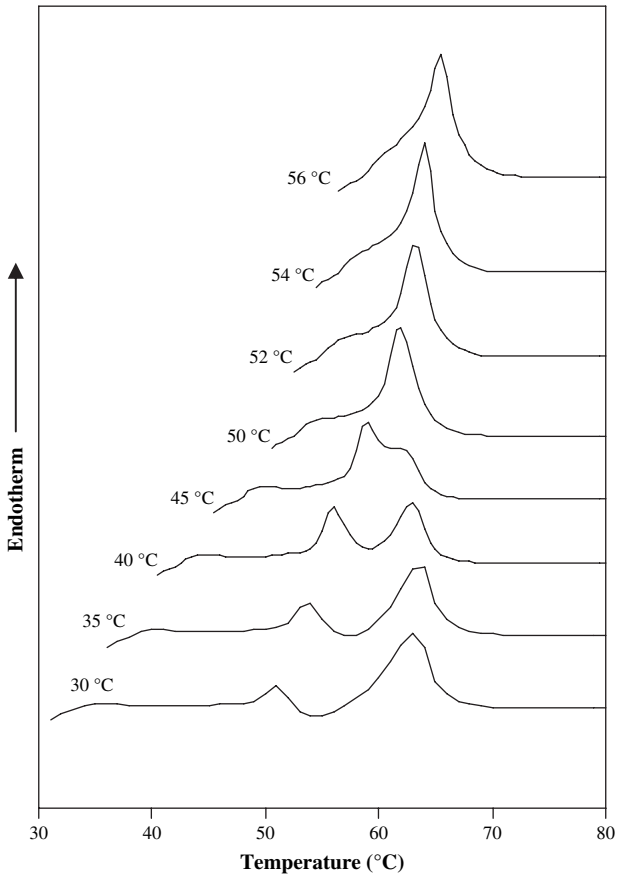

Fig. 2. DSC heating runs (20 °C/min) of poly(Glc-*alt*-6HH) samples isothermally melt-crystallized at temperatures ranging from 30 °C to 56 °C.

sample (11 kJ/mol). A degree of crystallinity ranging from 32% to 18% or from 57% to 34% can be consequently determined assuming a heat of fusion of 34 kJ/mol or 19 kJ/mol for a 100% crystalline sample. These values are estimated by considering the group contribution theory and the data given by different authors (4 kJ/mol corresponds to the methylene groups, but values of 5 kJ/mol [15] and −2.5 kJ/mol [16] can be found for the ester groups). The polymer easily crystallizes from the melt, giving rise to a hot crystallization peak that is observed at 25 °C in the cooling run performed at −10 °C/min. Note also that the polymer crystallizes during quenching since no exotherm is observed prior to the lamellar reorganization process in the subsequent heating run. The glass transition temperature is observed at −36 °C, well below room temperature.

The melting behavior of samples isothermally hot crystallized between 30 °C and 56 °C for long enough to reach the end of crystallization is shown in Fig. 2. The temperature of the first peak increases with crystallization temperature T_c, whereas the second peak always appears at a constant value (64 °C). The relative areas of these two peaks also depend on T_c, becoming the first peak dominant at high T_c. This behavior indicates that the first peak represents the melting of as-crystallized lamellae, whereas the second peak represents the melting of reorganized crystals, presumably crystallized during scanning. When T_c is increased, the initial lamellae are thicker to start with, melt at a higher temperature thus not allowing sufficient time for recrystallization of second peak lamellae, and leading to a decreased endotherm for high-T_c samples. The total melting enthalpy is measured by adding the areas associated with the two possible melting peaks and subtracting, if observed, the area of the exotherm associated with reorganization. This enthalpy slightly increases with crystallization temperature and varies from 6.9 kJ/mol for the sample crystallized at 30 °C to 8.5 kJ/mol for that crystallized at 56 °C. The estimated degree of crystallinity assuming the van Krevelen group contribution data [16] for such isothermally crystallized samples increases from 36% to 44%.

In order to analyze the crystallization kinetics, it is necessary to determine the equilibrium melting point (T_m^0) of poly(Glc-*alt*-6HH). Only the temperature of the first melting peak is considered since, as explained above, it represents the melting temperature of the as-crystallized material. A theoretical equilibrium melting temperature close to 77 °C (Fig. 3) is graphically determined according to the method developed by Hoffman and Weeks [17] (i.e., extrapolation of the plot of T_m versus T_c to $T_m = T_c$) when the data for the thinner crystals, which are formed at T_c, are considered.

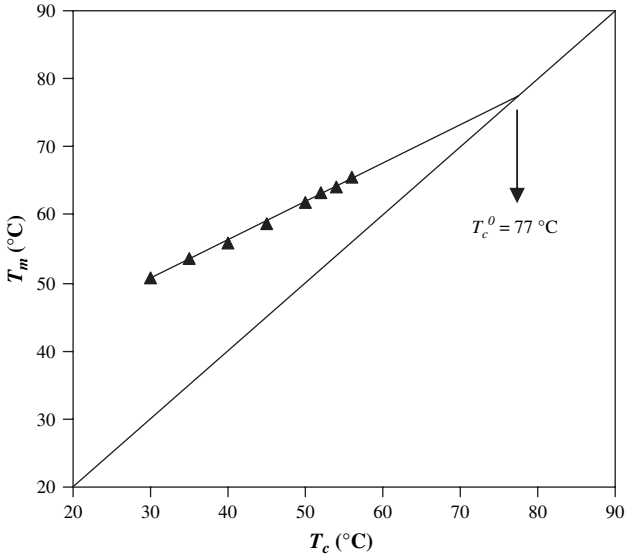

Fig. 3. Hoffman–Weeks plot of the temperatures corresponding to the first (▲) endothermic melting peak versus crystallization temperature. An equilibrium melting temperature close to 77 °C is deduced.

3.2. DSC study of the isothermal crystallization kinetics of poly(Glc-alt-6HH)

A crystalline weight fraction, $\chi(t)$, is obtained from the hot-crystallization DSC exotherms of poly(Glc-*alt*-6HH) by the ratio between the partial area at time t and the total exotherm area:

$$\chi(t) = \int_{t_0}^{t} (\mathrm{d}H/\mathrm{d}t)\mathrm{d}t \Big/ \int_{t_0}^{\infty} (\mathrm{d}H/\mathrm{d}t)\mathrm{d}t \qquad (1)$$

where $\mathrm{d}H/\mathrm{d}t$ is the heat flow rate and t_0 is the induction time. The crystallization exotherms become flat and shift to longer times with increasing hot-crystallization temperature.

The development of crystallinity for hot-isothermal crystallizations (Fig. 4a) shows a characteristic sigmoidal dependence on time. Unfortunately, temperatures below 35 °C are not suitable for reliable isothermal crystallization experiments because the sample begins to crystallize before the set T_c can be reached.

Kinetic crystallization data were analyzed assuming the Avrami equation [18–20] for the primary crystallization:

$$1 - \chi(t) = \exp[-Z(t - t_0)^n] \qquad (2)$$

where Z is the temperature-dependent rate constant and n is the Avrami exponent whose value varies according to the crystallization mechanism. This mechanism is composed of two steps: nucleation, which can be either homogeneous or heterogeneous depending on the way that nuclei are formed, and crystal growth.

A normalized rate constant, $k = Z^{1/n}$, is usually evaluated for comparison purposes since its dimension (time^{-1}) is independent of the Avrami exponent value.

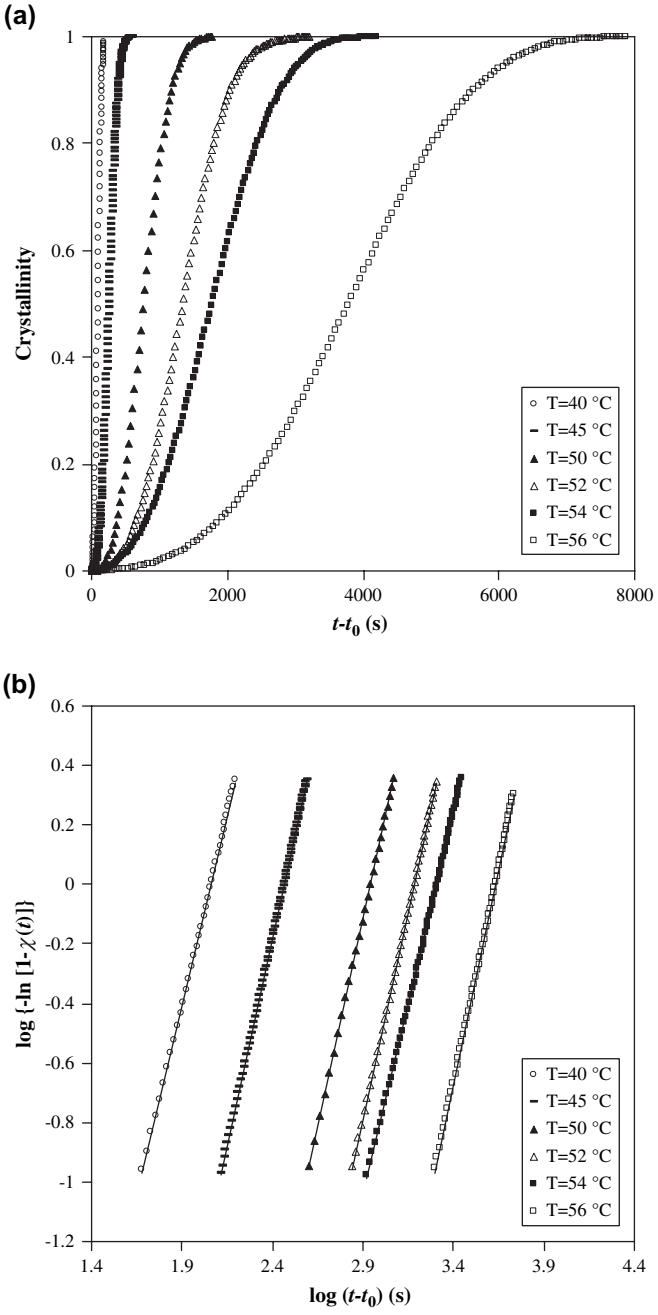

Fig. 4. (a) Development of crystallinity with time for different isothermal crystallizations performed between 40 °C and 56 °C. (b) Avrami analyses for the studied hot crystallizations of poly(Glc-*alt*-6HH).

The plots of $\log\{-\ln[1 - \chi(t)]\}$ against $\log(t - t_0)$ at different crystallization temperatures give straight lines (Fig. 4b) with slopes corresponding to the Avrami exponents and intercepts at $\log(t - t_0) = 0$ equal to $\log Z$. Table 1 summarizes the main kinetic parameters of the primary process and shows an Avrami exponent with a mean value of 2.70. A predetermined (heterogeneous) nucleation with spherical growth geometry can be assumed from the calculated Avrami exponents, the ideal value of n for such situation being 3. We discard the possibility of a sporadic (homogeneous) nucleation and disk-like growth geometry since such a situation is expected to occur at

Table 1
Isothermal hot crystallization parameters of poly(Glc-*alt*-6HH)

T_c (°C)	n	Z (s^{-n})	k (s^{-1})	$1/t_{1/2}$ (s^{-1})		
				DSC	WAXD	SAXS
35	2.44	7.46×10^{-5}	2.03×10^{-2}	2.52×10^{-2}	2.13×10^{-2}	1.67×10^{-2}
40	2.57	5.11×10^{-6}	8.73×10^{-3}	2.22×10^{-2}	1.02×10^{-2}	9.17×10^{-3}
45	2.79	1.35×10^{-7}	3.45×10^{-3}	9.92×10^{-3}	5.73×10^{-3}	5.88×10^{-3}
50	2.77	7.26×10^{-9}	1.15×10^{-3}	1.31×10^{-3}	3.40×10^{-3}	2.98×10^{-3}
52	2.80	1.22×10^{-9}	6.55×10^{-4}	7.49×10^{-4}		
54	2.57	3.11×10^{-9}	4.90×10^{-4}	5.60×10^{-4}		
55					8.47×10^{-4}	6.53×10^{-4}
56	2.89	3.06×10^{-11}	2.30×10^{-4}	2.62×10^{-4}		

large supercoolings and for thin films. Note that the samples were melt-crystallized inside the aluminium pans used for DSC analysis, and are consequently rather thick. In addition, a spherulitic morphology was observed for the melt-crystallized samples by polarizing microscopy, as will be described below.

The values of the normalized rate constant for the studied crystallization temperatures are summarized in Table 1 together with the reciprocal crystallization halftime ($1/t_{1/2}$). This parameter can be easily obtained from DSC experiments and reflects the overall rate of crystallization because it includes both nucleation and growth components [21]. A similar evolution of the two parameters with the crystallization temperature is found, a fact that supports the Avrami analysis performed. Both parameters increase when the crystallization temperature decreases, as is characteristic of a temperature region where crystallization is more controlled by nucleation than by molecular transport.

Next we analyze the overall rate of crystallization in terms of crystallization regimes. For a dominant heterogeneous nucleation it has been assumed that the Hoffman and Lauritzen equation [22] can be reformulated using the reciprocal crystallization halftime [23–25] ($1/t_{1/2}$) or the normalized constant [26–29] (k) instead of the radial growth rate (G) determined by hot stage optical microscopy experiments.

We have specifically considered the derived equation for the normalized constant:

$$k = k_0 \exp[-U^*/R(T_c - T_\infty)]\exp\left[-K_g/(T_c(\Delta T)f)\right] \qquad (3)$$

where k_0 is a constant preexponential factor, U^* represents the activation energy characteristic of the transport of crystallizing segments across the liquid–crystal interface, T_∞ is the temperature below which such motion ceases, T_c is the crystallization temperature, R is the gas constant, K_g is a nucleation parameter, ΔT is the degree of supercooling measured as $T_m^0 - T_c$, and f is a correction factor accounting for the variation in the bulk melting enthalpy per unit volume with temperature ($f = 2T_c/(T_m^0 + T_c)$).

The corresponding Lauritzen and Hoffman plot displayed in Fig. 5 shows that the data fit well with a straight line that is indicative of a single crystallization regime within the considered crystallization temperature interval. Values of $U^* = 1500$ cal/mol and $T_\infty = T_g - 30$ K give rise to a correlation coefficient, r, of 0.990 and a nucleation constant of 0.85×10^5 K^2, as deduced from the slope of the lineal fit.

Note that the U^* and T_∞ parameters correspond to those reported by Suzuki and Kovacs [30], which are values usually considered when isothermal crystallization is studied far above the glass transition temperature. In this case, the indicated parameters hardly affect the temperature dependence of the rate constant (nucleation control versus transport control), and standard values are usually employed.

Only one kind of spherulites is observed in the isothermal crystallizations of poly(Glc-*alt*-6HH) performed between 30 °C and 55 °C, a fact that is in agreement with the single crystallization regime detected in the indicated temperature interval. A fibrilar texture with the Maltese cross and negative birefringence is characteristic. Fig. 6 shows the morphologies attained at the lowest and the highest assayed crystallization temperatures. Spherulites have a small size because of the high nucleation rate, and consequently it is impossible to accurately analyze the crystal growth. Diameters reach only well measurable values close to 50 μm at the highest crystallization temperature when the nucleation rate is still comparable with the growth rate. The number of spherulites increases when the crystallization temperature decreases, but remains constant

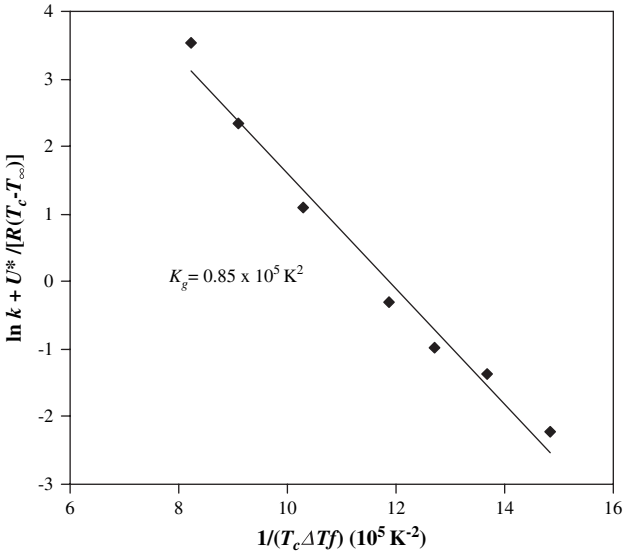

Fig. 5. Plot of $\ln k + U^*/R(T_c - T_\infty)$ versus $1/T_c(\Delta T)f$ to estimate the nucleation parameter K_g of poly(Glc-*alt*-6HH).

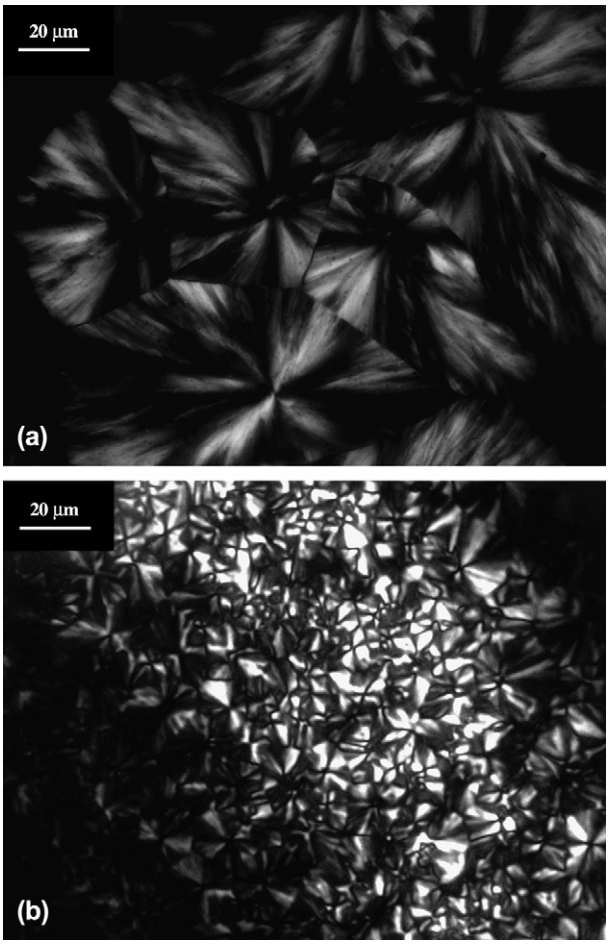

Fig. 6. Polarized optical micrographs of poly(Glc-*alt*-6HH) spherulites isothermally crystallized at 55 °C for 300 min (a) and at 30 °C for 30 min (b).

during crystallization, as is characteristic of an athermal process.

3.3. Study on the isothermal crystallization of poly(Glc-alt-6HH) by time-resolved SAXS/WAXD experiments

Fig. 7 shows representative time-resolved SAXS and WAXD profiles developed during isothermal crystallization at 50 °C and 55 °C, respectively. An SAXS long periodicity peak is clearly seen at a value of the scattering vector, $q = [4\pi/\lambda]\sin(\theta)$, close to 0.04 $Å^{-1}$ after subtraction of the empty sample background. The indicated long period peak can be attributed to the lamellar structure in the spherulites and starts to appear at a time that increases with the crystallization temperature. Subsequently the peak intensity increases significantly with time until reaching a plateau value. The initial WAXD profiles show only one amorphous halo whose intensity decreases when crystallization takes place, and on which Bragg reflections form. $(11\bar{1})$, (110), and (020) correspond to the most intense and significant reflections of a structure defined by a monoclinic unit cell having $a = 6.65$ Å, $b = 8.04$ Å, $c = 21.5$ Å and $\beta = 133°$. The intensities of these reflections increase significantly during the beginning of crystallization

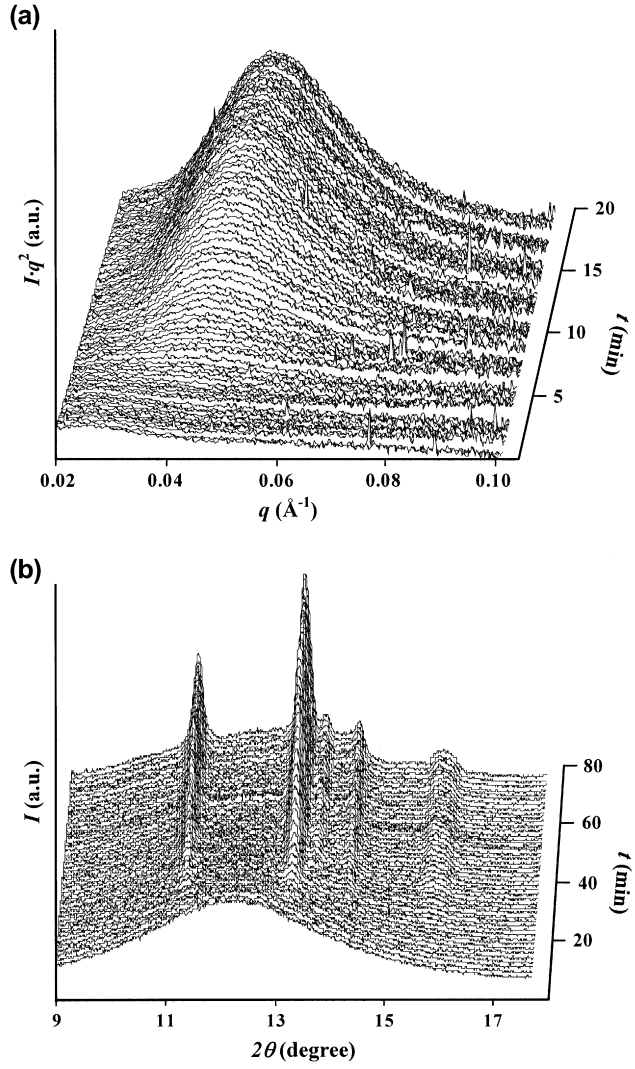

Fig. 7. Time-resolved SAXS (a) and WAXD (b) three-dimensional profiles of poly(Glc-*alt*-6HH) during isothermal crystallization at 50 °C (a) and 55 °C (b). SAXS curves are shown after subtraction of empty sample background and Lorentz correction.

until reaching their maximum values after a short time interval. For a given crystallization temperature, the SAXS long periodicity peak and crystal diffractions appear simultaneously, as expected for a crystallization process controlled by nucleation and crystal growth. Final SAXS profiles collected at different temperatures are shown in Fig. 8a. It can be clearly seen that the SAXS peak shifts to lower q values at higher crystallization temperatures, which corresponds to larger long spacings of the lamellar stacks.

SAXS data can be analyzed considering the normalized one-dimensional correlation function [31], $\gamma(r)$, which corresponds to the Fourier transform of the Lorentz-corrected SAXS profile:

$$\gamma(r) = \int_0^\infty q^2 I(q)\cos(qr)\mathrm{d}q \Big/ \int_0^\infty q_2^I(q)\mathrm{d}q \qquad (4)$$

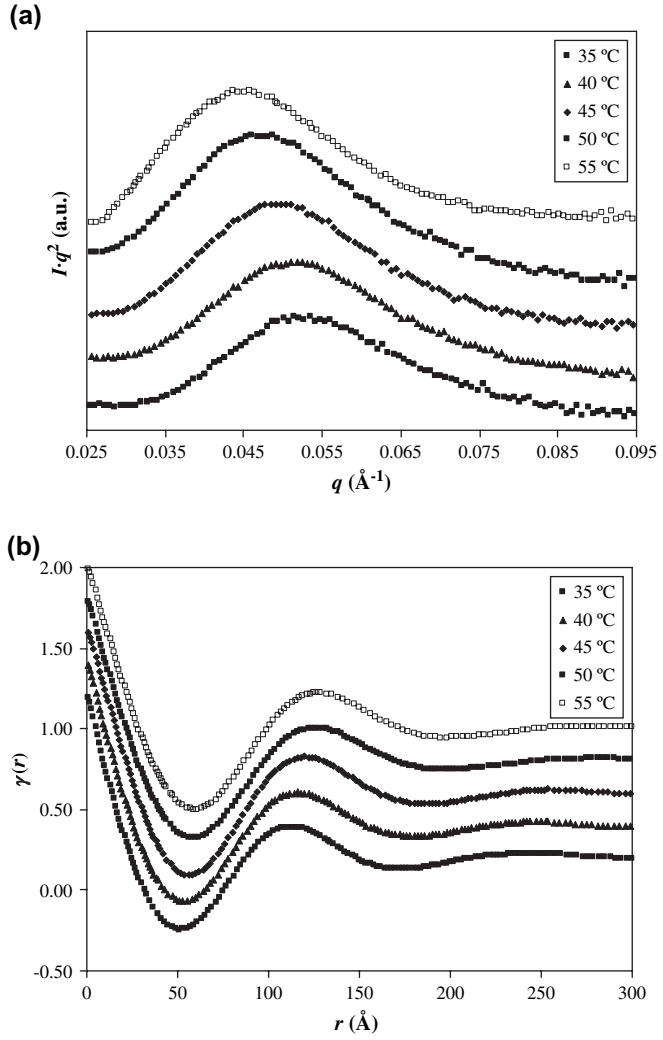

Fig. 8. The final SAXS profiles (a) and the corresponding correlation functions (b) at different crystallization temperatures for poly(Glc-*alt*-6HH).

Integrations must be carried out over the range of $0 < q < \infty$. Thus, extrapolations of the scattering intensity to both low and high q values are necessary since SAXS data were only collected in a limited angular range.

The former extrapolation has little effect on the correlation function because of the q^2 weighting. It has been performed using the Vonk model [32], which assumes an intensity profile defined by:

$$I(q) = H_1 - H_2 q^2 \tag{5}$$

where H_1 and H_2 are constants.

The second extrapolation to high q is carried out considering Porod's law:

$$I(q) = I_b(q) + K/q^4 \tag{6}$$

where I_b is the background intensity and K is the Porod constant.

Fig. 8b shows the correlation functions calculated for the final SAXS profiles obtained at different crystallization temperatures. Analysis of the correlation function allows to determine: (1) the long period, L_γ; (2) the crystallinity within the lamellar stacks, X_c^{SAXS}; (3) the crystalline lamellar, l_c, and the amorphous layer thickness, l_a; and (4) the scattering invariant, Q. In this way, L_γ corresponds to the r value of the first maximum of the correlation function; l_a has been assigned to the r value for the intersection of the LRAT (linear regression in the autocorrelation triangle) with the ordinate equal to the first minimum of the correlation function; l_c corresponds to $L_\gamma - l_a$; and X_c^{SAXS} is calculated as l_c/L_γ. The lower thickness of the two-phase lamellar model has been assigned to the amorphous layer thickness although the correlation function cannot distinguish the thickness associated with each phase. This fact will be then explained and has been well reported for other polymers [33–36].

The time evolution of the morphological parameters during isothermal crystallization at a representative temperature of 55 °C is shown in Fig. 9. This evolution shows a typical behavior where the invariant Q exhibits a sigmoidal increase with time. After the induction time, t_1, the SAXS profile starts to show a peak which grows continuously at a rapid rate. The primary crystallization develops between t_1 and the time at which the secondary crystallization starts, t_2. During the primary crystallization stage, both the average long period, L_γ, and the average lamellar thickness, l_c, have a significant decrease, as well established for other polymers like poly(ether ether ketone) [36]. During the secondary crystallization the indicated distances remain practically constant. The change in the interlamellar amorphous layer thickness, l_a, is significantly smaller than those indicated for L_γ and l_c. However, an increase of l_a during the primary crystallization is clearly observed. The changes in the morphological parameters, i.e., the sharp initial decreases of L_γ and l_c during the primary crystallization are consistent with the formation of new crystals at a rate for which the thickening of existing lamellae is comparatively negligible. The new secondary lamellae are inserted within the loosely stacked bundles of the primary lamellae and conduce to a denser stacking and a decrease of L_γ. Moreover, new lamellae suffer spatial restrictions

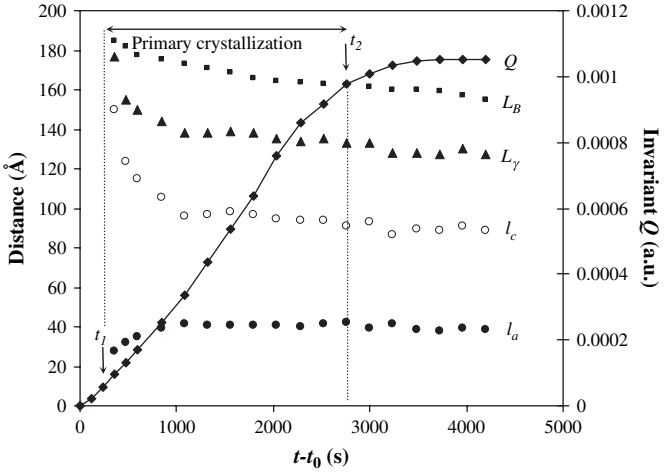

Fig. 9. Time evolution of the Bragg spacing, L_B, long period from correlation function, L_γ, crystal thickness, l_c, amorphous thickness, l_a, and scattering invariant, Q, during isothermal crystallization for poly(Glc-*alt*-6HH) at 55 °C.

leading to thinner defective crystals which account for the changes observed in l_c and l_a.

As usual [37], the Bragg long period, L_B, is larger than the L_γ value associated with the most probable distance between the centers of gravity of two adjacent crystals. A long period determined from twice the value of the first minimum of the correlation function, L_γ^m, is also useful since it is interpreted as the most probable distance between the centers of gravity of a crystal and its adjacent amorphous layer. The results obtained with poly(Glc-*alt*-6HH) show that L_γ is larger than L_γ^m for all crystallization temperatures, a fact that indicates a broader distribution of the layer widths of the major component [36], which in this case corresponds to the crystal phase.

Fig. 10 displays the invariant Q with time at different temperatures. An Avrami-like behavior is observed during the primary crystallization stage and after that a slight increasing Q value is determined during the secondary crystallization. The observed changes are rather similar to those determined by DSC for the evolution of the degree of crystallinity depicted in Fig. 4a. In fact, the time corresponding to a value of 0.5 for the invariant at each crystallization temperature can be measured and the corresponding reciprocal parameter, $1/t_{1/2}$, determined. These values are summarized in Table 1 and plotted in Fig. 11 together with those deduced from the DSC analysis. The fastest crystallization rate corresponds to the lowest studied T_c. The observed temperature dependence covers the right side (low supercooling region) of the characteristic bell-shaped kinetic curve, where crystallization is mainly controlled by nucleation. A rather good agreement is observed between DSC and SAXS results in spite of the temperature gap that may exist, indicating a strong parallel between the overall rate of crystallization and the lamellar growth since the kinetics for these two processes are comparable.

Fig. 12 shows the change in morphological parameters with crystallization temperature. It is clear that the long period increases when the crystallization temperature is raised. Thus, L_γ changes from a value of 111 Å at 35 °C to 129 Å at 55 °C. In fact, the mobility of polymer chain segments increases with temperature, and consequently the reorganization into larger chain-folding lamellae becomes enhanced. Both lamellar and amorphous layer thicknesses increase with temperature in a rather similar way. Increments close to 7 Å and 11 Å are detected in the considered temperature range for l_c and l_a, respectively.

The full width of half maximum of the SAXS peak, ω, decreases with crystallization time (Fig. 13) until a rather constant value is reached at the end of the primary crystallization. This fact indicates that the ordering of crystalline lamellae within the stacks reaches its maximum. The variation of the peak width with crystallization temperature (Fig. 13) is practically insignificant although a decreasing trend is detected, which suggests that the lamellar distribution becomes slightly narrower.

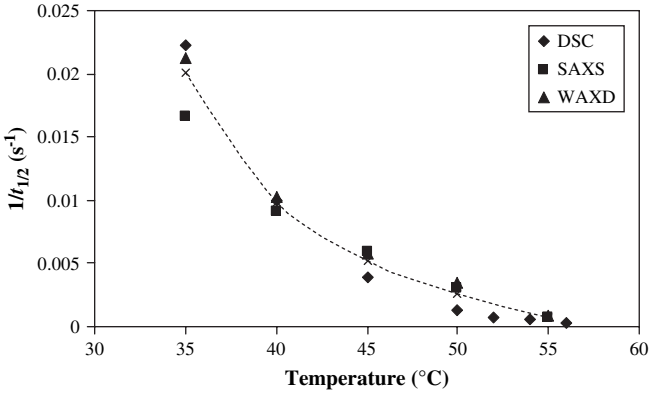

Fig. 11. The reciprocal crystallization halftimes determined by DSC, SAXS and WAXD at different temperatures for poly(Glc-*alt*-6HH). Trend line obtained with the averaged data from the three experiments is also drawn.

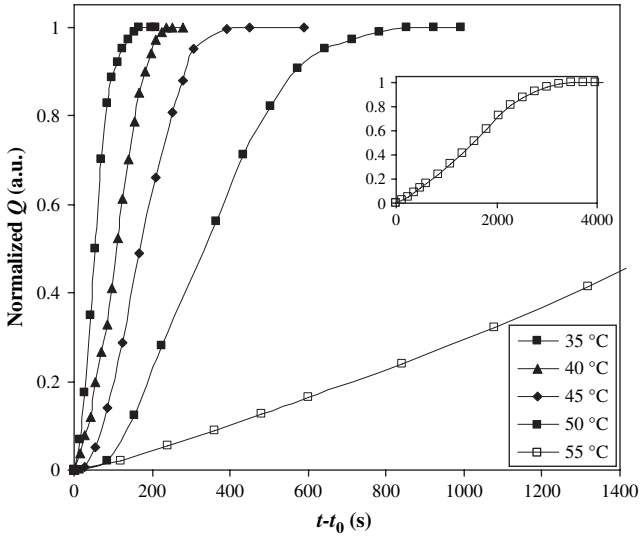

Fig. 10. Time evolution of the normalized SAXS scattering invariant Q at different temperatures for poly(Glc-*alt*-6HH). Inset shows complete data for the long time crystallization performed at 55 °C.

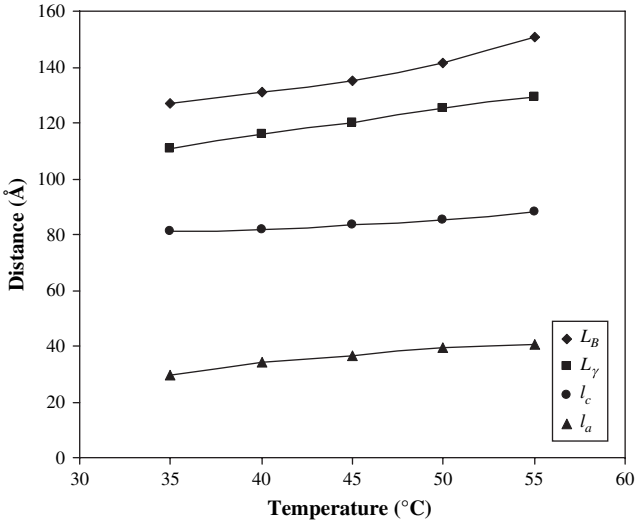

Fig. 12. Final SAXS Bragg spacing, L_B, long period from correlation function, L_γ, crystal thickness, l_c, and amorphous thickness, l_a, at various temperatures for poly(Glc-*alt*-6HH).

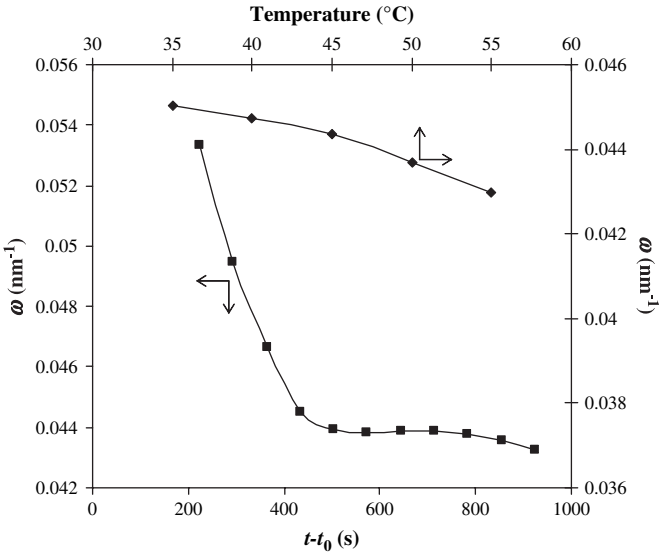

Fig. 13. Dependence of the full width at half maximum of the Lorentz-corrected SAXS peak upon crystallization time (■) and crystallization temperature (◆). Data correspond to a crystallization temperature of 50 °C (■) or the final SAXS profiles (◆).

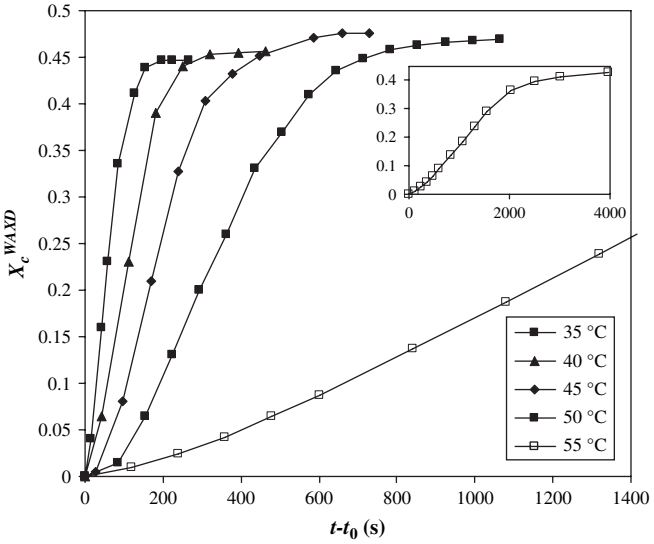

Fig. 15. Time evolution WAXD crystallinity, X_c^{WAXD}, at different temperatures for poly(Glc-*alt*-6HH). Inset shows complete data for the long time crystallization performed at 55 °C.

The final WAXD profiles of poly(Glc-*alt*-6HH) measured at different temperatures are shown in Fig. 14. The integrated intensity for each crystal reflection and amorphous background can be measured for the different time-resolved spectra obtained during each isothermal crystallization. A Gaussian–Lorentzian peak riding on a baseline is used to fit the amorphous background, and all other crystal reflection peaks are also fitted with Gaussian–Lorentzian functions. By dividing the total intensities of the crystalline reflections I_c by the overall intensity I_T, a measure of the mass fraction of the crystalline phase in the sample can be obtained. This value, X_c^{WAXD}, can be termed as the apparent mass crystallinity since, owing to possible distortions in the crystal lattice and thermal disorder, the measured value of I_c might underestimate the true value of crystallinity.

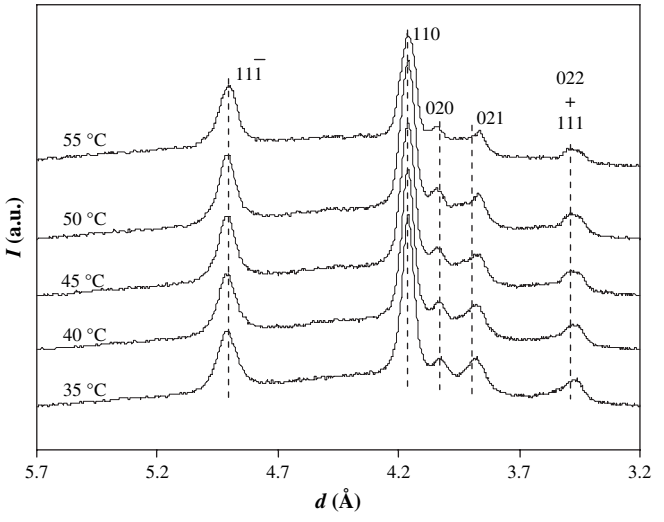

Fig. 14. Final WAXD profiles at different crystallization temperatures for poly-(Glc-*alt*-6HH).

The evolution of the WAXD crystallinity with time at different crystallization temperatures is displayed in Fig. 15. These crystallinity profiles become very similar to the evolution of the SAXS invariant profile, Q, and consequently show an Avrami-like growth behavior during the primary crystallization stage at all chosen temperatures. A practically constant crystallinity value is then reached during the secondary crystallization process. Final crystallinity slightly increases from 45% to 47% (Fig. 15) when crystallization temperatures vary from 35 °C to 45 °C. Final crystallinity values are difficult to determine at higher temperatures because of the long time required by secondary crystallization to be completed. WAXD crystallinities (ca. 45%) are in good agreement with those estimated by DSC using the van Krevelen group contribution theory [16] (ca. 40%).

The reciprocal crystallization halftimes deduced from WAXD experiments are summarized in Table 1 and plotted versus the crystallization temperature in Fig. 11. A good agreement is clearly found between the different methods (DSC, SAXS and WAXD) used to evaluate this kinetic parameter. In fact, the Hoffman and Lauritzen equation can be applied using all the reciprocal data (Fig. 16) and the same conclusions obtained with the analysis based on the normalized kinetic constant, k, are reached. Thus, the plot is defined by a single slope representative of one crystallization regime. The correlation coefficient and the nucleation constant become $0.981 \times 10^5\ K^2$ and $0.83 \times 10^5\ K^2$ when the U^* and T_∞ parameters are equal to 1500 cal/mol and $T_g - 30$ K, respectively.

Combined SAXS and WAXD data can be used to verify the assignment of the l_a and l_c thicknesses. Thus, the ratio between X_c^{SAXS} and X_c^{WAXD} is an estimate of the volume-filling fraction of the lamellar stacks, X_S. This value lies between 0.6 and 0.7

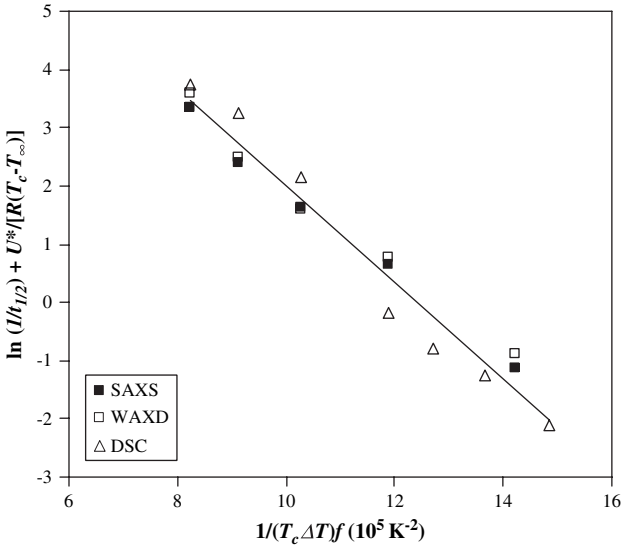

Fig. 16. Plot of $\ln(1/t_{1/2}) + U^*/R(T_c - T_\infty)$ versus $1/T_c(\Delta T)f$ to determine the nucleation parameter K_g for poly(Glc-*alt*-6HH). Reciprocal halftimes deduced from DSC, WAXD and SAXS experiments were considered to obtain the average line plot.

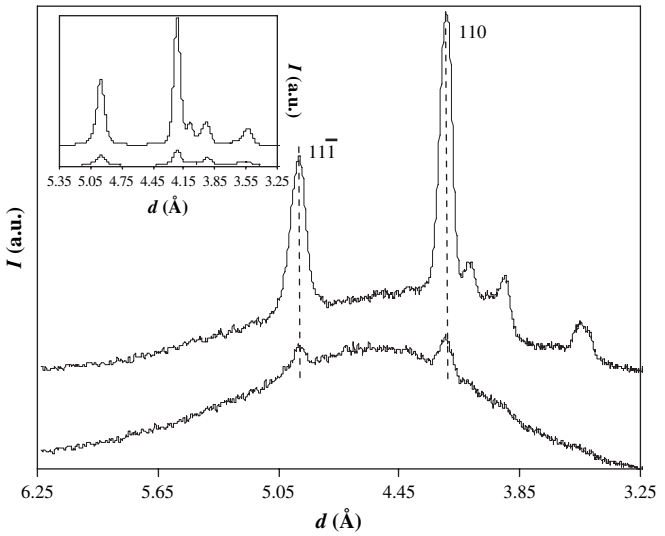

Fig. 18. WAXD profiles at the early (1320 s) and final (4200 s) stages of the isothermal crystallization performed at 55 °C for poly(Glc-*alt*-6HH). Inset shows the profiles obtained after elimination of the amorphous halo determined by deconvolution.

within the studied temperature range and indicates the existence of amorphous phase domains between the lamellar stacks. Note that the volume-filling fraction is larger than unity when the values of l_a and l_c are interchanged. As a result, a value without a physical meaning is attained with the wrong thickness assignment.

Comparison of the time evolution of the relative SAXS invariant, Q^{SAXS}, with X_c^{WAXD} shows that the two magnitudes are proportional to each other during the primary crystallization, whereas the change in X_c^{WAXD} becomes larger during secondary crystallization. This is more evident when the isothermal crystallization temperature decreases (Fig. 17) and is a consequence of the increase in the fraction of crystals within the lamellar stacks. This variation is highly significant in secondary crystallization and small (when compared to the variation in the fraction of lamellae within crystalline aggregates) in the primary crystallization.

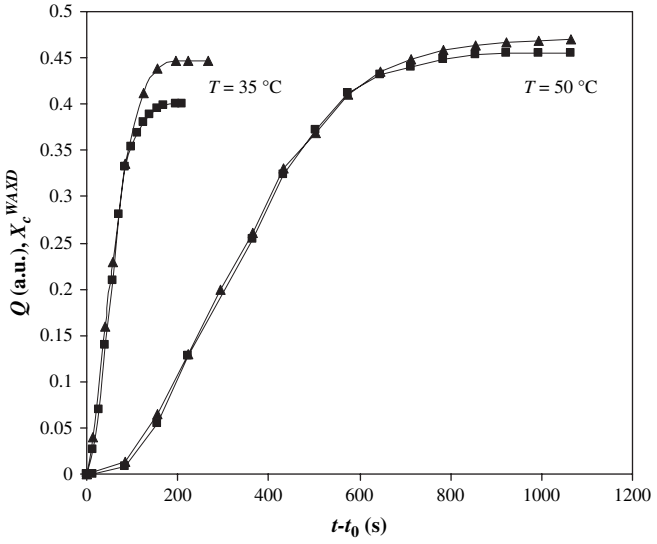

Fig. 17. Changes in Q^{SAXS} (■) and X_c^{WAXD} (▲) during isothermal crystallization at two representative temperatures.

The spacings of the strongest peak reflections remain practically constant during each isothermal crystallization, as shown, for example, in Fig. 18. Thus, cell parameters do not change significantly when the sample crystallizes at a given temperature. However, a slight decrease in full width at half maximum (δ_{hkl}) of the corresponding peaks is detected, and therefore the domain dimensions in the direction perpendicular to the *hkl* planes increase. Thus, the crystallization performed at 55 °C shows an increase in the $L_{11\bar{1}}$ and L_{110} domains from 25 nm to 35 nm and from 33 nm to 50 nm, respectively, according to the Scherrer equation, $L_{hkl} = 1/\delta_{hkl}$. Lamellar morphologies with large lateral dimensions agree with the observed narrow *hk*0 and *hkl* (with low *l*) peaks.

WAXD profiles obtained at the final stages of the crystallizations performed at different temperatures do not reveal a significant peak broadening (Fig. 15). Thus, crystalline domains are similar in the studied temperature range (35–55 °C). Spacings of *hk*0 reflections also remain constant and consequently the *a* and *b* unit cell parameters do not change. However, the spacings of the *hkl* reflections decrease with increasing temperature, which suggests a shortening of the chain axis parameter (from 21.5 Å to 20 Å) if a constant value is assumed for the monoclinic angle and the shift of the 021 reflection is considered. Temperature favours a slight deviation from the characteristic *trans* conformation, giving rise to a slightly tight molecular conformation.

4. Conclusions

The calorimetric studies performed with the sequential polyester derived from glycolic acid and 6-hydroxyhexanoic acid, poly(Glc-alt-6HH), indicate that the polymer is highly

crystalline (ca. 40%), has a well defined glass transition temperature at around −36 °C and a complex melting behavior. Thus, a double melting peak indicative of crystalline reorganization during heating may be detected. An equilibrium melting temperature of 77 °C is determined by the Hoffman and Weeks plot.

For the isothermal hot crystallization process, the values of the Avrami exponent range between 2.4 and 2.9, suggesting heterogeneous nucleation and three-dimensional spherulitic growth. This has also been confirmed by optical microscopy observations which revealed the formation of small Maltese cross spherulites. These are athermally nucleated, have a fibrillar texture and a negative birefringence.

Hot crystallizations performed between 35 °C and 56 °C show a single crystallization regime when the Lauritzen and Hoffman treatment is applied. An activation energy of the transport process and a nucleation parameter of 1500 cal/mol and $0.83-0.85 \times 10^5$ K^2, respectively, are deduced considering both the normalized kinetic constant and the reciprocal halftime. DSC, SAXS and WAXD experiments render consistent reciprocal halftime values.

SAXS and WAXD peaks appear simultaneously during isothermal crystallizations, indicating that the predominant growth mechanism is nucleation and crystal growth. Both long period and lamellar thickness decrease with crystallization time and then reach a plateau value at the final stage of crystallization. New crystals within loosely stacked lamellar bundles seem to be formed at a rate for which the thickening of existing primary lamella is comparatively negligible. Differences between SAXS and WAXD crystallinities suggest the existence of a significant amorphous fraction located between the lamellar stacks.

Acknowledgements

This research has been supported by CICYT and FEDER (grant MAT2006-02406). We want to express our gratitude to Drs. François Fauth and Ana Labrador of the BM16 station of ESRF for his help with the synchrotron experiments.

References

[1] Langer R. Nature 1998;392:5.
[2] Pentti U, Rokkanen P, Böstman O, Hirvensalo E, Mäkelä EA, Partio EK, et al. Biomaterials 2000;21:2607.
[3] Marler JJ, Upton J, Langer R, Vacanti JP. Adv Drug Delivery Rev 1998; 3:165.
[4] Chu CC. Wound closure materials and devices. Boca Raton, FL: CRC; 1997. p. 65–106 [chapter 5].
[5] Schmitt EE, Polistina RA. U.S. Patent 3,297,033; 1967.
[6] Bezwada RS, Jamiolkowski DD, Lee I, Agarwal V, Persivale J, Trenka-Benthin S, et al. Biomaterials 1995;16:1141.
[7] Vera M, Rodríguez-Galán A, Puiggalí J. Macromol Rapid Commun 2004;25:812.
[8] Vera M, Franco L, Puiggalí J. Macromol Chem Phys 2004;205:1782.
[9] Martínez-Palau M, Franco L, Ramis X, Puiggalí J. Macromol Chem Phys 2006;207:90.
[10] Chu CC. J Appl Polym Sci 1981;26:1727.
[11] King E, Cameron RE. J Appl Polym Sci 1997;66:1681.
[12] Zong XH, Wang ZG, Hsiao BS, Chu B, Zhou JJ, Jamiolkowski DD, et al. Macromolecules 1999;32:8107.
[13] Rueda DR, García-Gutiérrez MC, Nogales A, Capitán MJ, Ezquerra TA, Labrador A, et al. Rev Sci Instrum 2006;77: Art. No. 033904 Part 1.
[14] http://www.ccp13.ac.uk/software/program/corfunc/corfunc.htm.
[15] Davids DJ, Misra A. Relating materials properties to structure. Lancaster: Technomic Publishing Co.; 1999.
[16] van Krevelen DW. Properties of polymers: their correlation with chemical structure, their numerical estimation and prediction from additive group contribution. 3rd ed. Amsterdam: Elsevier; 1990.
[17] Hoffmann JD, Weeks JJ. J Chem Phys 1962;37:1723.
[18] Avrami M. J Chem Phys 1939;7:1103.
[19] Avrami M. J Chem Phys 1940;8:212.
[20] Avrami M. J Chem Phys 1941;9:177.
[21] Hoffman JD, Davis GT, Lauritzen JI. In: Hannay NB, editor. Treatise on solid state chemistry. New York: Plenum; 1976 [chapter 7].
[22] Lauritzen JI, Hoffman JD. J Appl Phys 1973;44:4340.
[23] Philips PJ, Lambert WS. Macromolecules 1990;23:2075.
[24] Urbanovici E, Schneider HA, Cantow HJ. J Polym Sci Part B Polym Phys 1997;35:359.
[25] Hong PD, Chung WT, Hsu CF. Polymer 2002;43:3335.
[26] Chan TW, Isayev AI. Polym Eng Sci 1994;34:461.
[27] Fatou JG, Marco C, Mandelkern L. Polymer 1990;31:890.
[28] Lu H, Qiao J, Yang Y. Polym Int 2002;51:1304.
[29] Kenny JM, Maffezzoli A, Nicolais R. Termochim Acta 1993;227:83.
[30] Suzuki T, Kovacs AJ. Polym J 1970;1:82.
[31] Vonk CG, Kortleve G. Kolloid Z Z Polym 1967;220:19.
[32] Vonk CG. J Appl Crystallogr 1975;8:340.
[33] Hsiao BS, Gardner KH, Wu DQ, Chu B. Polymer 1993;34:3986.
[34] Ikada Y, Jamshida K, Tsuji H, Hyoan SH. Macromolecules 1987;20: 906.
[35] Kruger KN, Zachmann HG. Macromolecules 1993;26:5202.
[36] Hsiao BS, Wang Z, Yeh F, Yan G, Sheth KC. Polymer 1999;40:3515.
[37] Santa Cruz C, Stribeck N, Zachmann HG. Macromolecules 1991;24: 5980.